Imaging properties of supercritical angle fluorescence optics

Jörg Enderlein,[1,4,*] **Ingo Gregor,**[1] **and Thomas Ruckstuhl**[2,3]

[1]*III. Institute of Physics – Biophysics, Georg August University, 37077 Göttingen, Germany*
[2]*Physikalisch-Chemisches Institut, Universität Zürich, CH-8057 Zürich, Switzerland*
[3]*t.ruckstuhl@pci.uzh.ch*
[4]*http://www.joerg-enderlein.de*
[*]*enderlein@physik3.gwdg.de*

Abstract: In recent years, new optical systems have been developed with the ability to collect light at very high angles of emission, exceeding the critical angle of total internal reflection. Prominent examples are solid-immersion lenses and paraboloid collectors. These systems achieve high efficiencies in fluorescence detection which is an important issue for sensitive applications in analytical chemistry and biochemical assays. The exclusive collection of supercritical angle fluorescence (SAF) allows for the detection of evanescent modes and thus to confine the detection volume within one wavelength to an interface. For conventional optical systems with high numerical aperture a precise wave-optical theory of imaging was developed by Richards and Wolf in the fifties of the last century. However, their theory is not directly applicable to *non-imaging, strongly aberratic* light collection systems systems that collect a significant part of light above the critical angle. Here, we extend the theory to describe the optical properties of such systems.

© 2011 Optical Society of America

References and links

1. B. Richards and E. Wolf "Electromagnetic diffraction in optical systems II. Structure of the image field in an aplanatic system," Proc. Roy. Soc. London A **253**, 358–379 (1959).
2. E. Wolf, "Electromagnetic diffraction in optical systems I. An integral representation of the image field," Proc. Roy. Soc. London A **253** 349–357 (1959).
3. M. Born and E. Wolf, *Principles of Optics*, 6th ed. (Pergamon Press, 1987).
4. T. Ruckstuhl and S. Seeger, "Confocal total-internal-reflection fluorescence microscopy with a high-aperture parabolic mirror lens," Appl. Opt. **42**, 3277–3283 (2003).
5. S. M. Mansfield and G. S. Kino, "Solid immersion microscope," Appl. Phys. Lett. **57,** 2615–2616 (1990).
6. P. Török, P. R. Munro, and E. E. Kriezis, "Rigorous near- to far-field transformation for vectorial diffraction calculations and its numerical implementation," J. Opt. Soc. Am. A **23,** 713–722 (2006).
7. M. Foreman, R. Matthew, S. Sherif, P. R. T. Munro, and P. Török, "Inversion of the Debye–Wolf diffraction integral using an eigenfunction representation of the electric fields in the focal region," Opt. Express **16,** 4901–4917 (2008).
8. P. Török, P. D. Higdon, and T. Wilson, "On the general properties of polarised light conventional and confocal microscopes," Opt. Commun. **148,** 300–315 (1998).
9. M. Leutenegger, R. Rao, R. Leitgeb, and T. Lasser, "Fast focus field calculations," Opt. Express **14,** 11277–11291 (2006).
10. M. Leutenegger and T. Lasser, "Detection efficiency in total internal reflection fluorescence microscopy," Opt. Express **16,** 8519–8531 (2008).

11. W. Lukosz and R. E. Kunz, "Light emission by magnetic and electric dipoles close to a plane interface II. Radiation patterns of perpendicular oriented dipoles," J. Opt. Soc. Am. **67,** 1615–1619 (1977).

12. W. Lukosz, "Light emission by magnetic and electric dipoles close to a plane interface III. Radiation patterns of dipoles with arbitrary orientation," J. Opt. Soc. Am. **69,** 1495–1503 (1979).

13. T. Ruckstuhl, J. Enderlein, S. Jung, and S. Seeger, "Forbidden light detection from single molecules," Anal. Chem. **72,** 2117–2123 (2000).

14. J. Enderlein and T. Ruckstuhl, "The efficiency of surface-plasmon coupled emission for sensitive fluorescence detection," Opt. Express **13,** 8855–8865 (2005).

15. E. M. Lifshitz, L. D. Landau, and L. P. Pitaevskii, *Electrodynamics of Continuous Media: 8 (Course of Theoretical Physics)* (Butterworth Heinemann, 1984), Chap. X.

16. F. Goos and H. Hänchen, "Ein neuer und fundamentaler Versuch zur Totalreflexion," Ann. Physik **436,** 333–346 (1947).

17. T. Ruckstuhl and D. Verdes, "Supercritical angle fluorescence (SAF) microscopy," Opt. Express **12,** 4246–4254 (2004).

18. J. Ries, T. Ruckstuhl, D. Verdes, and P. Schwille, "Supercritical angle fluorescence correlation spectroscopy," Biophys. J. **94,** 221–229 (2008).

19. M. Bhmer, and J. Enderlein, "Orientation imaging of single molecules by wide-field epifluorescence microscopy," J. Opt. Soc. Am. B **20,** 554–559 (2003).

1. Introduction

A fundamental goal of physical optics is the characterization of the imaging properties of a given optical system. When dealing with imaging of non-coherent fluorescent sources, this is equivalent to calculating the image of single dipole emitters as a function of their position in sample space. For aplanatic optical systems with high numerical aperture, an exact wave-optical approach for calculating their imaging properties was laid down by Richards and Wolf in two seminal papers in the fifties [1, 2]. Their approach employs the particular property of aplanatic imaging systems to obey Abbe's sine condition [3]. Although their method can be also adapted for moderately aberratic optical systems, it becomes inapplicable for systems that are strongly violating Abbe's sine condition (or any other simple relationship between propagation angles in sample and image space, such as Herschel's condition [3]). Two such optical systems are of particular practical importance: light collection optics using parabolic mirrors [4] or solid-immersion lenses [5]. Such systems are far from being aplanatic, and collect a considerable amount of light above the critical angle of reflection (supercritical light detection), i.e. modes that are *non-propagating* in sample space but become propagating after tunneling into the glass of the optics (paraboloid glass segment, solid immersion lens). For this situation, there is no straightforward method available for computing the point spread function.

As far as we know, all previously described methods for calculating optical systems with high numerical aperture use the property that the imaging system is close to a perfect imaging system obeying Abbe's sine condition. This allows to derive, in a rigorous way, the field distribution in image space when the field distribution in the focal region of the sample space is known, see for example Ref. [7]. However, this approach fails when the involved optics cannot be described by some simple relationship between plane wave modes in sample space and in image space. In that case, one usually takes recourse to ray tracing. Ray tracing is a general technique from geometrical optics that parses rays of light through an optical system as they interact with the optical interfaces of its elements. It can be generalized to include polarization effects by associating with each ray an electric-field polarization vector, and tracking its change during each interaction of the ray with an optical interface. Even more, ray tracing can be combined with wave-optics in the sense of Richards and Wolf by associating the rays impinging on the image plane with electromagnetic plane waves. The method can then be used to calculate point spread functions and imaging properties of arbitrary optical systems [8–10]. However, ray tracing in this simple form becomes problematic when trying to trace modes that are *evanescent*, because for an evanescent mode there is no obvious association with a light ray! However, evanescent

modes are important for emitters that are located close to an optical interface of the imaging system. Then, a considerable amount of energy can be transferred into the optical system via evanescent modes, i.e. modes that are non-propagating within the medium of the emitter, but that transform into propagating modes above the critical angle of total internal reflection (TIR) within the optical system [11, 12]. For example, a fluorescing molecule in air or water located on or close to a glass surface emits a considerable part of its radiation as supercritical angle fluorescence (SAF) into the glass above the TIR angle [13, 17].

Thus, for an optical system which (i) does not allow for a simple relationship between modes in the front and in the back of the optics, such as Abbe's sine condition, and which (ii) collects a significant part of light from evanescent modes of an emitter, there does not exist a straightforward method of calculating its point spread function. To derive and describe such a method is the purpose of the present manuscript. This will be done by a combined ray tracing and wave-optical treatment of evanescent emission of electric dipole emitters. The method allows for modeling the imaging and light collection properties of non-aplanatic optical systems with high numerical aperture and evanescent wave collection such as SAF. The method is exemplified on the example of a parabolic collection optics.

2. Theory

The theoretical treatment will be divided into several steps. Firstly, we briefly recall the angular distribution of radiation, the phase and the polarization properties of an oscillating electric dipole close to an optical interface. Secondly, we develop a method how to assign to that emission a bundle of rays with correct distribution of propagation directions, phases and polarizations. This is the core and original part of our work. Thirdly, we give a brief description of the ray tracing and image calculation procedure.

2.1. Angular distribution of electromagnetic field in glass half space

Consider a molecule in air deposited on a glass surface. The general geometry of imaging such a molecule is depicted in Fig. 1.

Omitting any constant factors, the angular distribution of the electric-field amplitude $\mathbf{E}(\theta, \phi)$ generated by an oscillating electric dipole with orientation angles θ, ϕ along direction $\kappa = (\sin(\theta)\cos(\phi), \sin(\theta)\sin(\phi), -\cos(\theta))$ per solid angle $\sin(\theta)d\theta d\phi$ is given by [14]:

$$\mathbf{E}(\theta, \phi) = \sin \beta \left[\mathbf{t}_s E_s^{||}(\theta) \sin \phi + \mathbf{t}_p E_p^{||}(\theta) \cos \phi \right] + \mathbf{t}_p \cos \beta E_p^{\perp}(\theta), \tag{1}$$

$$E_p^{\perp}(\theta) = \frac{n_g w_g}{w_m} \frac{q}{n_m} T_p \exp(i w_m h), \tag{2}$$

$$E_p^{||}(\theta) = \frac{n_g w_g}{n_m} T_p \exp(i w_m h), \tag{3}$$

$$E_s^{||}(\theta) = \frac{n_g w_g}{w_m} T_s \exp(i w_m h), \tag{4}$$

where β is the polar angle of the molecule's emission dipole orientation; h its vertical distance from the glass surface; $\mathbf{t}_p$ and $\mathbf{t}_s$ are orthogonal unit vectors perpendicular to the direction of emission κ,

$$\mathbf{t}_s = \frac{\kappa \times \mathbf{e}_z}{|\kappa \times \mathbf{e}_z|}, \qquad \mathbf{t}_p = \mathbf{t}_s \times \kappa, \tag{5}$$

whereby $\mathbf{e}_z$ is a unit vector perpendicular to the surface; n_g and n_m denote the refractive index values of glass and air, respectively; and the $T_{p,s}(\theta)$ are Fresnel's transmission coefficients for
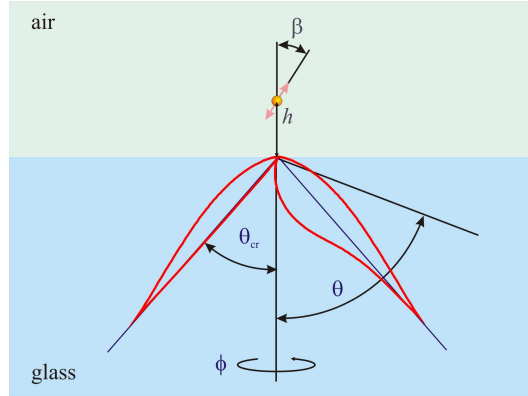
Fig. 1. Geometry of the emission of an electric dipole close to an interface: a single dipole emitter with an inclination angle β is placed at a distance h away from a glass surface. The angular distribution of radiation into the glass is depicted by the red solid line and is a function of angles θ and ϕ. Shown is a cross section of this function in a plane containing the optical axis (vertical) and the dipole axis. The critical TIR angle θ_{cr} between glass and air is also indicated by straight lines. It is important to realize that for plane wave modes above the TIR angle in the bottom medium, there are no corresponding propagating plane wave modes in the upper medium.

plane p- and s-waves through the air/glass interface traveling along direction κ into the glass, q is the in-plane component of the wave vectors, which is equal on both sides of the interface, and w_g and w_m are the z-components of the wave vectors in glass and air, respectively. Note that w_m (but not w_g) becomes purely imaginary for evanescent modes.

2.2. Virtual point of origin of light rays

The core task of this section is to obtain a relationship between the angular distribution of the electromagnetic field as derived in the previous subsection and a geometric ray representation of the emission that can be used for ray tracing. The central problem is as follows: it is straightforward to associate the emission from the dipole into subcritical angles of the glass, i.e. at angles below the TIR angle, with geometric rays of light by tracing a corresponding light ray starting at the dipole's position through the diffraction at the glass/air boundary into the glass. However, for supercritical angle emission at angles above the TIR angle, there is no such geometric ray interpretation, because this emission is related to evanescent modes that are non-propagating in air. Thus, one has to find a physically sound way for associating these emission modes in the glass with light rays. For finding a connection between light rays and emission direction, consider the electric field in the glass far away from the dipole's position. The phase $\Phi(\theta)$ of a pencil of light along emission angle θ with respect to a reference point given by the vertical projection of the dipole's position on the glass surface is given by

$$\Phi(\theta) = \arctan\left[\frac{|\Im\mathbf{E}|}{|\Re\mathbf{E}|}\right], \tag{6}$$

where $\mathbf{E}$ is the electric field amplitude vector as given by Eqs. (1) through (4). Please note that, due to symmetry reasons, $\Phi(\theta)$ is independent of the azimuthal angle ϕ of the emission. Thus, the phase along propagation direction with angle θ behaves as

$$\exp\left[ik_0 n_g(z\cos\theta + \rho\sin\theta) + i\Phi(\theta)\right]. \tag{7}$$

As a function of θ, this expression describes the wave front of the expanding light wave. The core idea is that each patch of the wave front is associated with a light ray that is perpendicular to the wave front's surface, i.e. perpendicular to the surface of constant phase [15]. Applying the principle of stationary phase one thus finds

$$k_0 n_g (-z \sin\theta + \rho \cos\theta) + \Phi'(\theta) = 0, \tag{8}$$

where a prime denotes differentiation with respect to θ. Thus, the virtual point of origin on the optical axis $\rho = 0$ of the corresponding patch of the wave front is located at

$$z_0(\theta) = \frac{\Phi'(\theta)}{k_0 n_g \sin\theta}. \tag{9}$$

As an example, we consider the case of a vertically oriented dipole (dipole axis along optical axis) sitting in air directly on the glass surface. The refractive index of air is $n_m = 1$, and that of glass is set to $n_g = 1.51$. For this situation, Fig. 2 shows the virtual distance z_0 as a function of emission angle in glass. For the dipole sitting directly on the glass surface, the functions $\Phi(\theta)$ and $z_0(\theta)$ are zero below the critical TIR angle.
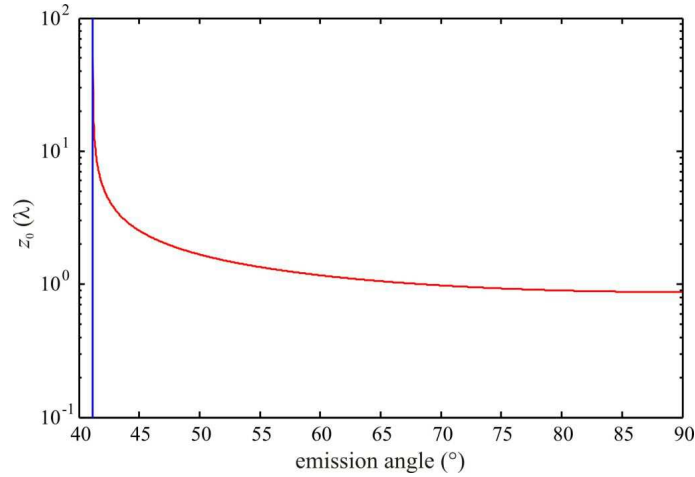

Fig. 2. Function $z_0(\theta)$ for a parallel (red line) and a vertically (blue line) oriented dipole on an air/glass interface. Vertical green line indicates the position of the TIR angle, where $z_0(\theta)$ diverges towards infinity. Notice that even in the limit $\theta \to 90°$, z_0 does not approach zero: the dipole seems to hover over the surface at a finite distance. This shift is a similar effect as the virtual lateral shift of the reflection point of a light beam upon TIR, the so-called Goos-Hänchen effect [16]. It should be noted that this figure will not change when moving the dipole away from the surface: For evanescent modes, the exponents in Eqs. (2) through (4) become real-valued, and the phase $\Phi(\theta)$, see Eq. (6), becomes independent on the dipole's position above the surface.

2.3. Image formation

Image formation is calculated by a hybrid ray-tracing and plane-wave approach. Let us consider the optical system as depicted in Fig. 3. A parabolic glass segment serves as light collector, collimating the emission from a dipole located at the focal point on its top surface by TIR on its lateral surface (glass/air interface). The parabolic shape of the segment is described by the equation $z = (\rho^2 - a^2)/2a$, where a is the radius of the planar top surface of the segment.

Collimated light that exits the glass segment at its bottom shall be refocused by an ideal lens with focal length f and axial position z_f towards a wide-field detector (camera). It should be noted that the z-axis (the optical axis) is not necessarily the same as the z-axis in the previous section, where it was passing through the dipole's position. In general, the dipole will have a laterally displaced position $(\rho_0 \cos\phi_0, \rho_0 \sin\phi_0, 0)$ with respect to the optical axis.
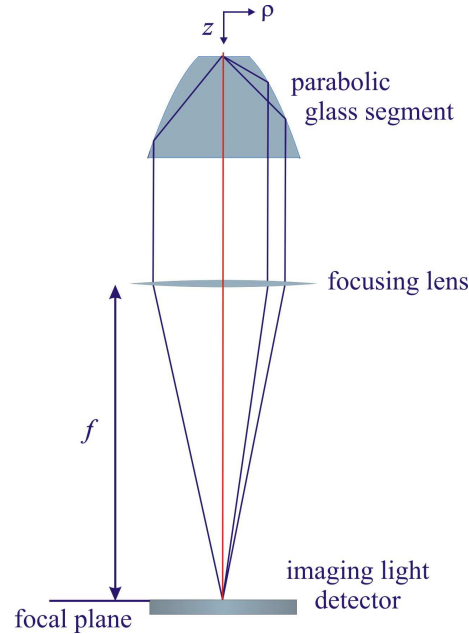

Fig. 3. Schematic of the parabolic light collection system.

The emission of a dipole into the glass segment is now considered to consist of bundles of light rays traveling into all possible directions, whereas a ray traveling along direction $(\sin\theta\cos\phi, \sin\theta\sin\phi, \cos\theta)$ starts at position

$$\mathbf{r}_0 = (z_0 \tan\theta \cos\phi + \rho_0 \cos\phi_0, z_0 \tan\theta \sin\phi + \rho_0 \sin\phi_0, 0), \tag{10}$$

having an initial optical phase

$$\psi_0 = \frac{k_0 n_g z_0 \sin^2\theta}{\cos\theta} + \Phi(\theta), \tag{11}$$

(see Eq. (7)) and an initial polarization equal to the polarization of $\mathbf{E}(\theta,\phi)$ in Eq. (1). For each ray, one performs a ray tracing of its subsequent propagation through the system (total internal reflection at paraboloid's lateral surface, refraction through segment's bottom surface, re-focusing by ideal lens towards the detector). During ray tracing, one records not only the position and direction of each ray, but also the change of the optical phase along its path and the re-orientation and attenuation of the associated electric field vector. This is done by handling all reflections and refractions as an interaction of a plane wave with a planar surface, thus taking into account also phase jumps upon TIR. In the image plane (position of the CCD detector), each light ray is finally associated with a plane wave traveling along the ray's direction with corresponding optical phase and polarization. Finally, the intensity distribution in the image plane is calculated as the absolute square of the superposition of all plane waves.

3. Results and discussion

In what follows, all lengths are given in units of the vacuum wavelength. As a concrete example, we consider the imaging properties of the paraboloid light collection system as shown in Fig. 3 with the following parameters: radius of top surface of the paraboloid glass segment $a = 10^4$, axial position and focal length of the refocusing lens are $z_f = -5 \cdot 10^5$ and $f = 10^6$, respectively. This reflects fairly well the parameters of existing paraboloid light collection setups. The refractive index of the glass segment was assumed to be 1.51, that of air was set to 1. We calculated the image of a dipole emitter positioned directly on the glass surface and considered three different dipole orientations along x, y and z and six dipole positions along x between $x_0 = 0$ and $x_0 = 5$ in steps of one. We further considered two different imaging conditions: (i) only supercritical angle fluorescence is collected, and (ii) light is collected only below the critical angle down to a collection angle of $\approx 30°$. The computational results are shown in Figs. 4 and 5.
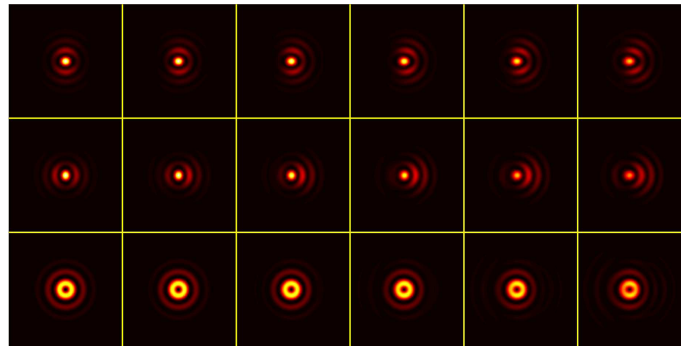

Fig. 4. Images of a dipole emitter on glass for SAF collection. Shown are results for three dipole orientations along the horizontal figure axis (top row), vertical figure axis (middle row), and an orientation perpendicular to the figure plane (along the optical axis, bottom row). From left to right, the images show six different lateral dipole positions, from $x_0 = 0$ till $x_0 = 5$ in steps of one. Each of the 18 images has an edge length of 300.
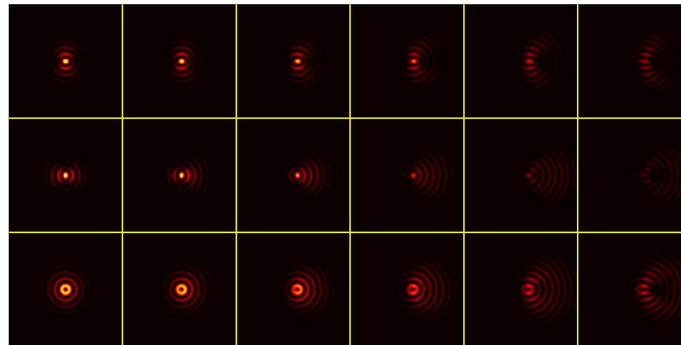

Fig. 5. Same as Fig. 4 but for "classical" light collection below the TIR angle.

First at all, the results show how sensitive the images are against lateral displacement of the emitter from the optical axis. For the on-axis position, refocusing of the emission light is best for sub-critical angle light collection and less efficient for SAF light collection. However, sub-critical angle collection is extremely sensitive against lateral displacement, which is shown

by the quick deterioration of the images with increasing displacement. It should be noted that the calculations are equivalent to calculating the point spread function (image of an isotropic emitter) of the system, which is obtained when adding the images for all three dipole orientations. When repeating the calculations for different axial dipole positions, one can obtain the three-dimensional molecule-detection function (MDF), which is of importance in Fluorescence Correlation Spectroscopy (FCS) [18]. Another potential application is defocused imaging of an emitter for determining its three-dimensional orientation in space [19]. As an example, we repeated the calculations of Figs. 4 and 5, but for an emitter on the optical axis and varying positions of the focal plane (by moving the image plane away from the focusing lens, see Fig. 3). The results for SAF as well as sub-critical light detection are shown in Fig. 7 and 6, respectively.
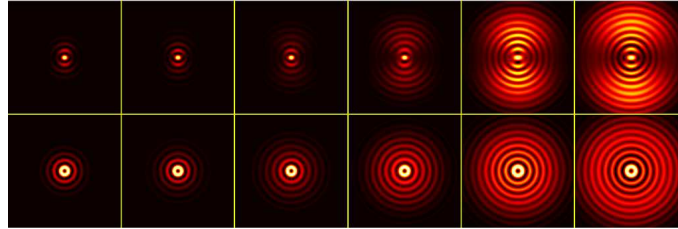

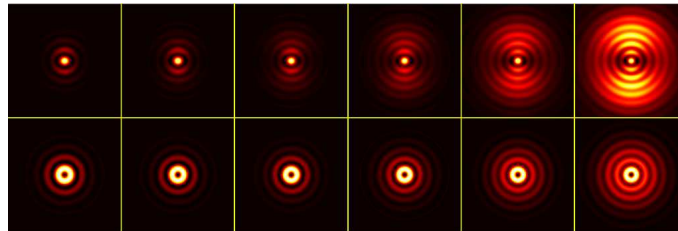Fig. 6. Same as Fig. 7 but for "classical" light collection below the TIR angle.

Fig. 7. Images of a dipole emitter on glass for SAF collection. Shown are results for two dipole orientations along the horizontal figure axis (top row), and for an orientation perpendicular to the figure plane (along the optical axis, bottom row). From left to right, the images show six different positions of the image plane away from the focal plane of the focusing lens, from $z = 0$ till $z = -40$ in steps of 8. As before, each of the 12 images has an edge length of 300.

4. Conclusion

We have presented a general approach for calculating the light collection/imaging properties for strongly aberratic systems which collect a significant part of light above the critical angle of TIR. One of the core results of our paper is given by Eq. (9), which determines the virtual origin of light pencils associated with a given patch of the wavefront in glass. We applied our general theoretical approach to imaging a dipole emitter with a parabolic light collection system.